Supplementary Information

Novel core-shell (TiO_2@Silica) nanoparticles for scattering medium in a random laser: higher efficiency, lower laser threshold and lower photodegradation.

Ernesto Jimenez-Villar*[a], Valdeci Mestre[b], Paulo C. de Oliveira[b] and Gilberto F. de Sá[c]

[a]*Instituto de Ciencia Molecular, Universitat de València. C/ Catedrático José Beltrán 2, Paternan46980, Spain. E-mail: Ernesto.Jimenez@uv.es*
[b]*Departamento de Física, Universidade Federal da Paraíba, João Pessoa, Paraíba58051-970, Brasil*
[c]*Departamento de Química Fundamental,Universidade Federal de Pernambuco, Recife 50670-901, Brazil*

Received (in XXX, XXX) Xth XXXXXXXXX 20XX, Accepted Xth XXXXXXXXX 20XX
DOI: 10.1039/b000000x

Materials

R6G laser dye ($C_{28}H_{31}N_2O_3Cl$), with molecular weight 479.02 g/mol, supplied by Fluka: Ethanol alcohol (C_2H_5OH) with spectroscopic grade purity, supplied by Alphatec: Tetra-ethyl-ortho-silicate (TEOS), supplied by Sigma-Aldrich. The titanium dioxide (TiO_2, nanoparticles 410 nm) of rutile crystal structure was acquired from DuPont Inc (R900).

Chemical synthesis of silica-coating on TiO_2 nanoparticles

In the first stage, 2 g of TiO_2 Np were diluted in 250 ml of absolute ethanol. The solution of TiO_2 nanoparticles was then divided into two equal portions of 125 ml. One of the parts was placed in a bath at 5 °C and 1.1 ml of TEOS, previously diluted in 11 ml of ethanol, was added. The 10% diluted solution of TEOS was added in 110 portions of 100 µl during the course of 1 hour. The solution was stirred during the TEOS addition. The other portion was stored and used as a reference in every experiment. Previously, before adding the TEOS, the solution of TiO_2 Np was placed in an ultrasound bath for 20 minutes to disperse the particles.

The TEOS hydrolysis and subsequent condensation of silica on the TiO_2 surface was provoked, taking advantage of the catalytic effect in the near surroundings of TiO_2 Np. [1,2] In addition, the possible accumulation of water molecules around the nanoparticles would favor TEOS hydrolysis. Probably, the electric potential associated with the surface of the nanoparticles themselves, in conjunction with the higher dielectric permittivity of the water, should promote the accumulation and polarization of water molecules in the vicinity of TiO_2 Np. [3] Self superficial hydrolysis of TiO_2 nanoparticles [4] would also favor the TEOS hydrolysis. The superficial irregularities of the TiO_2 nanoparticles must cause intensification of superficial electric potential in the regions with a smaller curvature radius. This phenomenon should increase the medium polarization, water accumulation and catalytic effects in these regions, leading to silica coating irregularities.

Characterization and sample preparation:

Transmission electron microscopy (TEM) was used on a 100kV JEOL, model 1200EX, microscope. The commercial carbon-coated Cu TEM grid was immersed in the solution of TiO_2@Silica nanoparticles that had previously been diluted 50-fold and then left to dry, before being introduced into the microscope. The stoichiometric ratio (Ti/Si) was determined by Energy Dispersive X-Ray fluorescence (ED-XRF) using an X-ray spectrometer SIEMENS D5000. The sample was prepared in three steps: precipitation, washing and drying. The nanoparticle powder (TiO_2@Silica) was pressed into a tablet form with a 12 mm diameter.

Experimental setup of random laser measurement

Supplementary Figure 1S shows a schematic diagram of the random laser (RL) experimental setup. The pumping source of the random laser was the second harmonic of a *Q*-switched Nd:YAG Continuum Minilite II (25 mJ, λ = 532 nm, with a pulse width of ~6 ns, repetition rate up to 15 Hz and spot size of 3 mm). The pump laser beam was incident upon the sample at 15 degrees. The laser power was regulated through neutral density filters (NDF), a polarizer and a half wave plate.

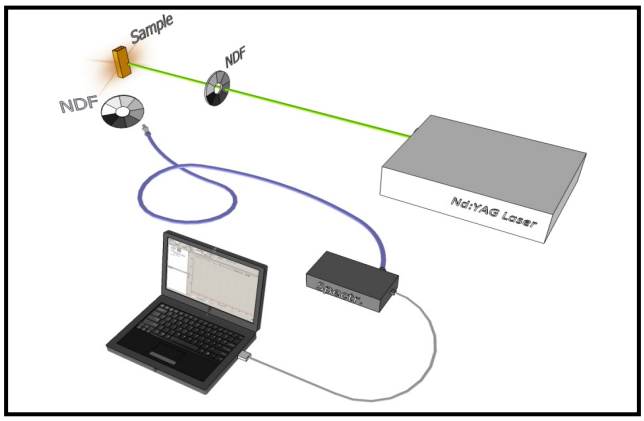

Supplementary Figure 1S. Schematic diagram of the RL experimental setup; NDF neutral density filter.

The samples were accommodated in a 2 mm path length quartz cuvette. The emission spectra were collected through a multimode optical fiber (200 µm), coupled to a spectrometer HR4000 UV-VIS (Ocean Optics) with a 0.36 nm spectral resolution (FWHM). The collection angle was ~60 degrees with respect to the sample surface, that is, 45 degrees with respect to the incident pumping beam. The liquid samples were placed in an ultrasound bath for about 10 minutes before recording the spectrum, in order to obtain the same dispersion of nanoparticles (initial conditions) in all measurements.

Random laser action

The pumping energy fluence varied between 0.12 and 120 mJ/cm^2 for the study of random laser action. This range of fluencies is below those used to study the photodegradation process (180 J/cm^2). Each value of emission intensity and bandwidth represented in the graphs (fig. 1c and d) was taken by integrating 10 laser pulses, which allowed us to rule out any photodegradation effects during the measurement.

Supplementary Figure 2**S** (a and b) shows two typical emission spectral curves for the dye solution for two kinds of nanoparticles (TiO_2, TiO_2@Silica) at 5.6x10^{10} Np/ml; the broad spectrum was obtained for excitation well below the laser threshold (0.24 mJ/cm^2), while the narrow spectrum was recorded

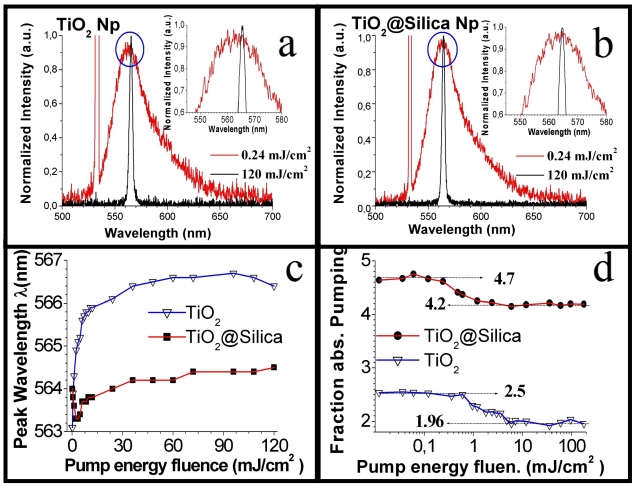

Supplementary Figure 2S. a-b) (Red online) Emission spectra below (broad band spectrum) and above (narrow band spectrum) the RL threshold: a) TiO_2 nanoparticles system and b) TiO_2@Silica system. Inside, it is shown the maximum emission peaks framed with blue circles. c-d) Influence of the pump energy fluence on: c) Peak wavelength of emission spectrums and d) fraction of absorbed pumping (FAP) (FAP values for fluencies well below FAP_{bT} and above FAP_{aT} RL threshold are embodied in the graphic). The scattering nanoparticle concentration was 5.6x10^{10} Np/ml and [1x10^{-4}M] for R6G.

for 120 mJ/cm^2. The peak intensities of the narrow and broad bands were normalized to show the narrowing effect more clearly. For the TiO_2 and TiO_2@Silica systems, the peak intensity relationship (narrow/broad) is 3.6 and >4 orders of magnitude larger, respectively. Note that the RL spectrum is redshifted, with respect to the center of the luminescence spectrum at low pump intensity of >3nm for the TiO_2 system. This shift was previously observed and explained by a model considering absorption and emission at the transition between the ground and the first excited singlet of the dye molecule. [5] The redshift of the RL spectrum is almost null (<0.5nm) for the TiO_2@Silica system. This effect should be due to the fact that the ratio between R6G molecules and R6G molecules involved in the stimulated emission is close to unit [R6G]/[$R6G_{stimulated}$]≈1 at 120 mJ/cm^2, which is evidenced in a higher efficiency of the RL (TiO_2@Silica). The peak position of the emission spectrum was measured as a function of the pumping energy fluence (between 0.12 and 120 mJ/cm^2). Figure 2S (c) shows a comparison of these peak positions with fluence for the TiO_2@Silica and TiO_2 systems. The emission spectrum shows a redshift for the TiO2 system, which undergoes a large increase in fluence between 0.12 and 12 mJ/cm^2 (0 to 2.8 nm). This redshift increases slightly (between 3 and 3.6 nm) for fluencies >12 mJ/cm^2. Instead, the emission spectrum peak for TiO_2@Silica system shows a blueshift for fluencies ≤12 mJ/cm2. For fluencies between12 mJ/cm^2 and 120 mJ/cm^2, the redshift increases in the same fashion, from 0 up to ~0.5 nm.

Figure 2Sd shows the fraction of absorbed pumping $\left[FAP = \left(I_{RNp}/I_{RNp+R6G}\right) = 1/e^{-l_{eO}/l_a}\right]$ as a function of energy fluence for the two systems (TiO_2@Silica, TiO_2). The parameters l_{eO} and l_a are the average photon path length and ballistics absorption length, respectively. The FAP values at fluencies well below (FAP_{bT}) and above the (FAP_{aT}) RL threshold are constants for either system (TiO_2, TiO_2@Silica). The FAP value decreases for fluencies from 0.24 mJ/cm^2 up to 2.4 mJ/cm^2 (TiO_2@Silica). For the TiO_2 system, the FAP value decreases for higher fluencies from 0.6 mJ/cm^2 up to 4.8 mJ/cm^2. This effect should be associated with a decrease in R6G molecules in the ground state S_0 and/or the population increment at S_i excited singlet states, which requires higher fluencies for the TiO_2 system. The fast process of vibrational relaxation of R6G molecules (~2ps) prevents a greater drop in FAP values (FAP_{bT}/FAP_{aT}). The ratio between photon residence time (τ_{eO}) and the vibrational relaxation times (τ_{R6G}) of R6G molecules (τ_{eO}/τ_{R6G}) should determine the relationship between FAP values, before and above the RL threshold(FAP_{bT}/FAP_{aT}).

Colloidal stability and scattering mean free path measurements

The above results of RL action could be associated with a more colloidal stability of TiO_2@Silica nanoparticles, which would represent a higher effective scattering surface. It is known that silica nanoparticles have a higher colloidal stability than those of TiO_2. [6, 7] The issue related to the colloidal stability of the scattering medium has not been discussed much in regards to the treatment of RLs. The authors of these papers do not take into account the effects of agglomeration of the particles that compose the scattering media, which would significantly change the scattering mean free path (l_s), a crucial parameter in the operation of RLs. Additionally, the electrical interaction between rhodamine molecules and nanoparticle components of the scattering medium should increase local concentration of rhodamine around the nanoparticles, affecting the colloidal stability. The fact that the counterion of the rhodamine is much heavier than Cl^-, would cause a decrease of the zeta potential associated with the TiO_2 nanoparticles (negative), approaching zero.

Experimental setup for scattering mean free path measurements

For suspensions of two different concentrations (5.6x10^{10} Np/ml and 8.9x10^{11} Np/ml) of TiO_2 and TiO_2@Silica, we determined the scattering mean free path from the transmission experiment.[8] Figure 3Sa shows a schematic diagram of the scattering mean free path measurement. The transmitted intensity I_t was determined as a function of slab thickness: the laser beam (second harmonic of *Q*-switched Nd:YAG Continuum Minilite II, λ = 532

nm, 1 μJ (1mJ attenuated 10^3 times by neutral density filters), with a pulse width of ~6 ns, repetition rate 10 Hz) was passed through a positive lens L_1 (200 mm focal length) so as to obtain the focus with its waist near the pinhole PH_1 (600μm diameter). The cell consisted of two optical flat F in wedge form, in this way; the slab thickness depends on the incidence point of the cell. Another pinhole, PH_2 (1200μm diameter), was positioned 80 mm away to PH_1 in order to reduce the diffuse light. Yet another lens, L_2 (50 mm focal length), allowed focalization of the coherent light on the optical fiber (200μm). Figure 3Sb and c shows typical curves of TiO_2@Silica samples (concentrations $5.6x10^{10}$ Np/ml and $8.9x10^{11}$ Np/ml) versus slab thickness.

	(TiO_2@Silica)		(TiO_2)	
Concentrations (Np/ml)	$5.6x10^{10}$	$8.9x10^{11}$	$5.6x10^{10}$	$8.9x10^{11}$
l_s values **(μm)**	**20.6±0.2**	**2.1±0.04**	**52±4**	**15±1**

Supplementary Table 1S. l_s values determined by transmission experiment for the TiO_2@Silica and TiO_2 systems at two nanoparticle concentrations ($5.6x10^{10}$ Np/ml and $8.9x10^{11}$ Np/ml).

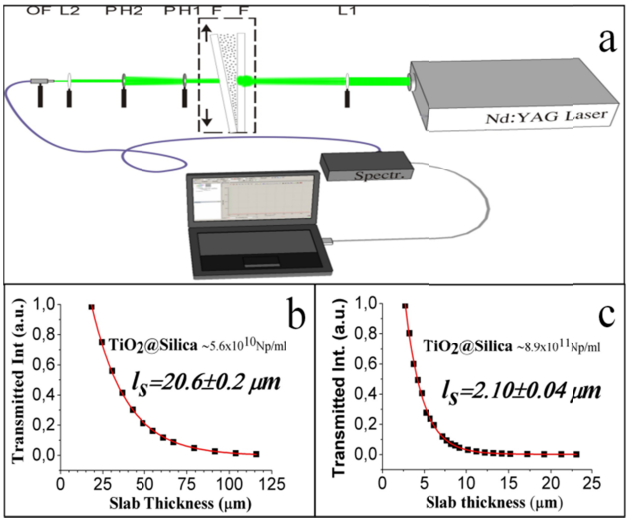

Supplementary Figure 3S. a) Schematic diagram of the experimental setup for the determination of transmitted intensity as a function of slab thickness. L_1 and L_2, lens; F+F, cell consisting in two optical flat mounted on a translation stage; PH_1 and PH_2, pinholes; OP, optical fiber to collect the light in the spectrometer. b-c) typical curves of transmission light versus slab thickness for the TiO_2@Silica system: b) for [$5.6x10^{10}$ Np/ml], l_s determined was 20.6±0.2 μm, c) for [~$8.9x10^{11}$ Np/ml], l_s determined was 2.1±0.04 μm. The red solid lines correspond to the fitted exponential functions.

FAP_{bT} values allow us to determine the average photon path length (pumping light) ($l_{eO} = l_a * \ln[FAP_{bT}]$). In this way, the average number of scattering events undergone by each N_i incident channel before being reflected could be determined from l_{eO} values. Each N_i channel of a pumping beam would be scattered an average of N_d times in volume $V_{l_s} \approx {l_s}^3$, where $N_d = l_{eO}/l_s$ and V_{l_s} is a cube with sides equal to l_s. The channel numbers that propagate N_P through area A_{ls} at λ=532nm (TiO_2@Silica), could be estimated by:

$$N_p = (20.6\mu m)^2/(0.532\mu m)^2 \approx 1500\ channels.$$

For the TiO_2@Silica system and [$5.6x10^{10}$ Np /ml] (FAP_{bT}=4.7):

$$l_{eO} = 885\mu m * \ln(4.7) \approx 1370\mu m \text{ and}$$
$$N_d = 1370\mu m/20.6\mu m \approx 66 \ll 1500.$$

Therefore, if $N_d \ll N_p$, it would mean that interferential events are highly unlikely. For the sample containing TiO_2 nanoparticles at [$5.6x10^{10}$ Np /ml] (FAP_{bT}=2.5):

$$l_{eO} = 885\mu m * \ln(2.5) \approx 810\mu m,$$
$$N_p = (52.4\mu m)^2/(0.532\mu m)^2 \approx 9700\ channels \text{ and}$$
$$N_d = 810\mu m/52.4\mu m \approx 15 \ll 9700.$$

However, the concentration and refractive index of the samples are similar. The specular reflections are similar for both systems (TiO_2 and TiO_2@Silica), so the coupling of pumping radiation to the samples is the same. Notice that, at this concentration, the particle volume represents < 1% of the samples. Therefore, from these facts it can be inferred that we are in the presence of two colloidal systems with different stabilities (TiO_2@Silica>TiO_2). This means that the effective concentration of TiO_2 nanoparticles is lower, suggesting the formation of agglomerates. In other words, the effective scattering surface is lower in the TiO_2 system. Even when the TiO_2@Silica nanoparticles agglomerate, the effective scattering surface would be preserved, unlike with TiO_2 nanoparticles.

Photodegradation studies

The photocatalytic pathway involves a reaction on the TiO_2 surface following several steps: 1) photogeneration of electron–hole pairs by exciting the semiconductor with >3.2 eV light, 2) separation of electrons and holes by traps existing on the TiO_2 surface and 3) a redox process induced by the separated electrons and holes with the adsorbates present on the surface.

The exponential decrease of the RL intensity, for the system TiO_2, indicates that the photodegradation is proportional to its derivative, as to the photodegradation rate. This means that the charge transfer [9], and therefore the redox reaction, [10] will cause a greater charge transfer in the next laser shot. Thus, one might think that the high concentrations of charges created by the TiO_2 nanoparticles at high pumping fluencies must react with the proper surface of the nanoparticles, reducing Ti^{4+} and oxidizing O^{2-}. This process results in oxygen vacancies, [11] which act as traps for photoelectrons. These electrons, trapped near the surface, act as a source of electron transfer coming from these superficial traps, increasing the efficiency of the redox process. [12] Additionally, the creation of oxygen vacancies in TiO_2 causes a progressive decreasing of gap on the nanoparticle surfaces (TiO_2), which is reflected in the progressive increase in the creation of electron-hole pairs. This photo-darkening effect is observed in films of TiO_2 exposed to successive irradiation of laser pulses. [11,13]

The photodegradation process for the TiO_2@Silica system presents a linear behavior. However, the modulus of the slope increases slightly after the emission intensity decreases to 50%. This fact indicates that the photodegradation rate of R6G remains constant until the emission intensity decreases to 50%. Subsequently, the photodegradation rate experiences a slight increase, but remains constant. This phenomenon could be due to the decreased absorption of R6G, provoking an increase of the effective pumping fluence inside the scattering medium

(TiO_2@Silica), which should increase the photodegradation rate of R6G.

Photodegradation as a function of pumping fluence

In the sample containing TiO_2 nanoparticles, the photodegradation has an exponential-linear dependence with pumping fluence. The linear part corresponds to the region with low fluencies (< 140 mJ/cm^2) and the exponential component to that with high fluencies (>160 mJ/cm^2). This exponential behavior must be the result of a progressive increase in the degradation rate of the TiO_2 nanoparticle surfaces with fluence. This effect has been previously observed in films composed of TiO_2 nanostructures. [11,13] The linear behavior shows a photodegradation rate of a -4.9 ± 0.5 x10^{-3} mJ cm^{-2}/ shot, which is 3 times higher than that observed for the TiO_2@Silica system, however the $FAP_{aT(TiO2)}$ and $l_{s(TiO2)}$ are ~2.1 times smaller and ~2.5 times greater, respectively. Thus, one might think that the mechanisms of the RL photodegradation are different in the TiO_2 and TiO_2@Silica systems. The FAP_{aT} values (TiO_2 and TiO_2@Silica) decrease with increasing number of shots. For a very large number of shots, values tend to hover around 0.9 and 1 for TiO_2 and TiO_2@Silica systems, respectively. The FAP values should tend to 1 for the two systems; however, for the TiO_2 system, it tends to be at around 0.9. This is most likely because the effective pumping intensity is higher inside the sample without R6G. Therefore, the photodegradation rate of TiO_2 Np should be higher for the sample without R6G. Thus, after the R6G is degraded, the pumping intensity reflected by the TiO_2 scattering medium without R6G is lower than the one with R6G. This effect does not occur for the TiO_2@Silica system, because these nanoparticles do not undergo photodegradation. The photodegradation rate of R6G in the TiO_2@Silica system remains constant with the pumping fluence (-1.55 ±0.05 x10^{-3} mJ cm^{-2} /shots), which is similar to the one reported by Yamashita M. and Kashiwagi H. [14]

Higher particle concentration

For the TiO_2@Silica system, at this high Np concentration, the values obtained for the narrower bandwidth and laser threshold were 4.2 nm and 1.65 mJ/cm^2, respectively (Figure 3b). The laser threshold is lower than the obtained at lower nanoparticles concentration (1.81 mJ/cm^2), however, the bandwidth increases. Notice that the measure obtained with our experimental setup averaged over the irradiation (3mm diameter) and coherent emission areas at this high concentration should be around three orders lower. Moreover, it should be noted that the FAP value starts to decrease to fluencies >0.036 mJ/cm^2, which is less than those for lower Np concentrations (>0.24 mJ/cm^2). This could mean that, for higher particle concentrations, the population inversion could be achieved for lower fluencies (Figure 3c). RL action studies from micrometer-sized areas are in development, which could bring more clarity.

For the TiO_2 system at high fluencies (≥48 mJ/cm^2), the RL efficiency increases (Figure 3a) and the redshift of the RL emission peak decreases (Figure 3d). These effects could be associated with decreasing l_s, which would mean that the pumping energy is confined in a smaller volume. It is known that potent laser pulses induce disaggregation of particles, which would result in an effective increase in the Np density. For the lowest TiO_2 Np concentration, the fluencies per unit volume achieved within the sample should be insufficient to cause particle disaggregation.

The ABS_{aT} values ratio for [10^{-4}M] of R6G $\left(ABS_{(TiO2@Silica)}/ABS_{(TiO2)}\right)^{aT} = 0.48/0.19 = \mathbf{2.53}$ is higher than the one for a lower Np concentration, but it does not correspond to the RL_{effic} ratio (5.1±0.2). The inequality $\left(ABS_{(TiO2@Silica)}/ABS_{(TiO2)}\right)^{aT} \neq \left(Rl_{(TiO2@Silica)}/RL_{(TiO2)}\right)^{eff}$ could be caused by the decrease of fluorescence lifetime and the quantum efficiency of R6G molecules closer to the TiO_2 surface. For higher Np concentrations (8.9x10^{11}Np/ml), the R6G molecules must be a good deal closer to the TiO_2 surface, which favors the fast electron transfer into the conduction band of the TiO_2. An insulating silica shell (1-10nm) on the surface of the TiO_2 shields the R6G molecules from the semiconductor surface.[15]

FAP_{bT} values could determine the average number of scattering events, N_d, undergone by each N_i incident channel before being reflected. Thus, for the TiO_2@Silica system at [8.9x10^{11} Np/ml]:

$$N_d = 885\mu m * \ln(2.0)/2.1\mu m \approx 292 \text{ and;}$$

$$N_p = (2.1\mu m)^2/(0.532\mu m)^2 \approx 16 \ll 292$$

Therefore, if $N_d \gg N_p$, it would mean that the probability of interferential events can be increased. Despite that, at lower concentrations (5.6x10^{10} Np/ml), $N_d \approx 66 \ll N_p \approx 9700$, which means that interferential events are highly unlikely. For the TiO_2 system and high Np concentrations (~8.9x10^{11}Np/ml):

$$N_d = 885\mu m * \ln(1.36)/15\mu m \approx 18 \text{ and;}$$

$$N_p = (15\mu m)^2/(0.532\mu m)^2 \approx 795 \gg 18$$

On the other hand, the great redshift (5.4 nm) of the RL emission peak, together with saturated absorption and emission, could mean that the few R6G molecules in the ground state, S_0, exhibit an absorption band equivalent to that of a higher concentration. This phenomenon could be associated to interferential events, which could provoke an increase in the transition probability per unit time from ground state S_0 to S_i excited singlet states.

We should note that all measures, random laser action and FAP were repeated three times yielding the same results. Therefore, we can rule out any possible effect of photodegradation in the samples during measurement.

References

1 Rafi-ud-din, Qu Xuanhui, Li Ping, Lin Zhang, Wan Qi, M. Zubair Iqbal, M. Yasir Rafique, M. Hassan Farooq, and Islam-ud-din, *J. Phys. Chem. C* 2012, **116 (22)**, 11924–11938

2 Kamal Abderrafi, Ernesto Jimenez, T. Ben, S.I. Molina, R. Ibáñez, V. Chirvony, J.P. Martínez-Pastor, *J. Nanoscience and Nanotechnology* 2012, **12 (8)**, 6774-6778

3 A. Luzar, S. Svetina, and B. Zeks, *J. Chem. Phys.* **1985**, ***82***, 5146

4 Philippe Leroy, Christophe Tournassat, Mohamed Bizi, *Journal of Colloid and Interface Science* 2011, **356, (2)**, 442-453

5 M.A. Noginov, H.J. Caulfield, N.E. Noginova, P. Venkateswarlu, *Optics Communications* 1995, **118**, 430-437.

6 Yang Zhang, Yongsheng Chen, Paul Westerhoff, Kiril Hristovski, John C Crittenden, *Water Research* 2008, **42 (8-9)**, 2204–2212

7 Chih-ping Tso, Cheng-min Zhung, Yang-hsin Shih, Young-Ming Tseng, Shian-chee Wu an d Ruey-an Doong, *Water Science & Technology* 2010, **61 (1)**, 127-133
8 Martin B. van der Mark, Meint P. van Albada, Ad Lagendijk, *Physical Review B* 1988, **37 (7)**, 3575-3592.
9 Amy L. Linsebigler, Guangquan Lu, and John T. Yates, Jr. *Chem. Rev.* 1995, **95**, 735-758
10 Photocatalysis-Fundamentals and Applications; Serpone, N., Pelizzetti, E., Eds.; Wiley: *New York Chapter* **7,** van Damme, H. *Supports in Photocatalysis* 1989.
11 M. Tsukamoto, N. Abe, Y. Soga, M. Yoshida, H. Nakano, M. Fujita, J. Akedo, *Appl Phys A* 2008, **93**, 193–196
12 Heinz Ceriscber and Adam Heller**,** *The Journal of Physical Chemistry* 1991, **95 (13)**, 5261
13 Tsukamoto Masahiro, Shinonaga Togo, Takahashi masanari, Fujita Masayuki,· Abe Nubuyuki, *Transactions of JWRI* 2011, **40 (1)**, 21-23
14 Yamashita, M.; Kashiwagi, H., *IEEE Journal of Quantum electronics* 1976, **12 (1)** Part:1, 90-95
15 Lydia Bechger, A. Femius Koenderink, Willem L. Vos, *Langmuir* 2002, **18**, 2444-2447